Testing and simulation of a solar PV/battery storage system with and without PWM charge control

Wael Yassine and Kevin R. Anderson*

Department of Mechanical Engineering,
Solar Thermal Alternative Renewable Energy Lab,
California State Polytechnic University,
Pomona, CA 91768, USA
Email: waelyassine93@gmail.com
Email: kranderson1@cpp.edu
*Corresponding author

Abstract: This paper presents an experimental and modelling study of an off-grid solar photovoltaic system using pulse width modulation (PWM) charge control and battery storage using manganese oxide as the cathode, carbon titanium phosphate composite as the anode, and alkali-ion saltwater as the electrolyte battery cells. The paper presents an experimental test apparatus, empirical data collection and numerical modelling and simulation of the system. The experimental data for charging and discharging the system is used to correlate the numerical simulation model output. Results for charging and discharging the system are subsequently used to develop transfer function models of the system's charging and discharging behaviour.

Keywords: solar; photovoltaic; batteries; charge controller; simulation; experiment; modelling; energy storage; data acquisition; correlation; transfer function.

Reference to this paper should be made as follows: Yassine, W. and Anderson, K.R. (2020) 'Testing and simulation of a solar PV/battery storage system with and without PWM charge control', *Int. J. Renewable Energy Technology*, Vol. 11, No. 1, pp.86–110.

Biographical notes: Wael Yassine received his MS in Mechanical Engineering from California State Polytechnic University, Pomona, in 2018. His thesis was on solar energy, photovoltaic/battery systems with charge controllers. He has done research in the field of solar energy, in both photovoltaics and solar water heating systems. He earned his BE in Mechanical Engineering from the American University of Beirut in Lebanon, in 2016. This paper is based on the masters thesis research of Yassine, W. (2018).

Kevin R. Anderson is a Professor of the Department of Mechanical Engineering at California State Polytechnic University, Pomona, CA, USA. He received his BS in Mechanical Engineering in 1991 from California State Polytechnic University, Pomona, CA, USA and MS in Mechanical Engineering from University of Colorado at Boulder in 1994, and his PhD in Mechanical Engineering from University of Colorado at Boulder in 1998. His research area includes renewable energy technology advancement and development.

1 Introduction

This paper studies the effects of charge controllers on the performance of batteries charged from solar panels. This present is based on the work of Yassine (2018). The paper discusses the fabrication and testing of a Photovoltaic (PV)/battery/charge controller test facility used to develop charge/discharge history data which is subsequently used to develop Laplace Transfer functions of the charge and discharge portions of the operation of the PV/battery storage/charge controller system. The current work is in the context of previous work performed in the arena of testing, modelling and simulation of off-grid PV/battery storage systems using charge controller. Photovoltaic cells (PVC's) produce electric energy, which is then stored in batteries for use. However, in most cases, the voltage and current of the panels are greater than the capacity of the battery, which leads to the overcharge of the battery. Charging a battery with a voltage or current greater than what it can sustain will degrade it, causing its performance to drop and its life to decrease. In addition, even if the voltage and current output of the panels match those of the battery, supplying energy to the battery when it is fully charged will also degrade it and reduce its life and performance. During nighttime, when the panels cannot produce a current, a backflow current can occur from the battery to the panels, which causes discharge and loss of electric energy. To prevent overcharge, charge controllers are used to regulate the power input from the panel to the battery. A charge controller reduces the voltage output of the array of solar panels to that of the battery, which is usually 12 or 24 V. Also, the current output of the panel arrays is reduced to that which the battery can safely operate without overcharging. When the battery is fully charged, the charge controller will stop the power flow from the panels to the battery, thus preventing overcharge. Charge controllers also prevent backflow current, which keeps the stored energy saved for use. There are two basic types of charge controllers, pulse width modulation (PWM), and maximum power point tracking (MMPT). The PWM control strategy regulates the power input to the battery by sending pulses of voltage and current in certain time intervals. At the end the each pulse, the controller stops supplying power and measures the voltage in the battery. The controller will send out the next pulses of voltage and current depending on those measured from the battery. The sent voltage pulse is slightly greater than the battery voltage by about 0.5 V, which accounts for cable losses. The PWM controllers act as switches that supply energy at certain time intervals as pulses with constant value. The MMPT controllers use the maximum power output of the solar array to supply power to the battery. During the day, the maximum power of the panels will change depending on solar insolation and ambient temperature. At any given time, the panels will be giving a certain output power. The MMPT controller acts as a DC transformer where the product of voltage and current remains with same, but there are always minor power losses in this process. The power will be that of the input power of the array. Depending on the battery voltage, the output current will be the power output of the array divided by the battery voltage. This provides more current to safely charge of the battery, which increases the efficiency of the charge controller. The research and development work of PV/battery storage systems is still very active, as can be seen from the body of works discussed herein. The study of Verma and

Gupta (2016) presents a review of the modelling design and controlling function of solar photovoltaic (PV) grid connected systems from various sources available through literature. The research of Chen et al. (2012) used the state-space approach and presents the modelling of a complete photovoltaic (PV) inverter system. The work of Mirzaei et al. (2017) outlines the design and construction of a charge controller for stand-alone PV/battery hybrid system by using a new control strategy and power management. In the study of Jariso et al. (2017), the modelling and designing of stand-alone photovoltaic system in Ethiopia is presented. The work of Alvarez et al. (2017) presents the results of modelling a grid-connected PV/battery micro-grid System using an MPPT controller. The research of Barote et al. (2008) presents a stand-alone wind system with vanadium redox battery energy storage. The work of Glavin et al. (2008) outlines a stand-alone PV super-capacitor battery hybrid energy storage system. The research of Amor et al. (2015) presents a study for the economic and technical approach for a grid connected PV power system. The work of Das and Ashok (2018) presents a control strategy for power management of an isolated micro hydro-PV-Battery hybrid energy system. The controls work of Tazay and Zhixin (2018) presents control of a three-phase hybrid converter for a PV charging station. modelling and simulation of generic PV/Battery systems continues to attract interest in the literature. For instance, the work of Abbes et al. (2013) presents an advanced synthetic study on the systems and control aspects of modelling and simulation of a PV system. In Cai et al. (2016) the modelling, analysis and control design of a two-stage photovoltaic generation system is presented. The work of Prakash and Singh (2016) presents fundamental designing and modelling of solar PV Cell and array. The study of Shaw et al. (2016) outlines the modelling and control of a battery connected standalone PV system. In the particular area of using MATLAB/Simulink/SIMSCAPE for research, the paper of Tsai et al. (2008) present the development of generalised photovoltaic model using MATLAB/SIMULINK. The work of Miller and Wendlandt (2010) outlines real-time simulation of physical systems using Simscape, while the study of Shah and Biate (2016) presents the design and simulation of Solar PV Model Using MATLAB/Simulink. The work of Bellia et al. (2014) provides results for the detailed modelling of photovoltaic module using MATLAB. As illustrated in the above literature review, the area of PV/Battery storage system modelling and testing is an ongoing region of research and development. Each of the studies outlined above possess their own particular focus, idiosyncrasies, and nuances and all are value-added to the PV/Battery modelling and testing community of researchers and engineers. The objective of the current paper is to assemble/characterise by test/and model a PV/battery storage/charge controller/pump system. The particular system considered employs manganese oxide as the cathode, carbon titanium phosphate composite as the anode, and alkali-ion saltwater as the electrolyte for the battery cells. This current research is value-added since it uses experimental data to correlate a systems level frequency domain model of a typical off-grid PV/battery storage/charge controller/pump system. This data and model can be used in higher level systems engineering models to predict performance of such renewable energy systems using this type of PV/energy storage. The paper is outline as follows: presentation of the experiment test facility, testing and data collection for charge an discharge, modelling of charge and discharge by correlating the voltage, current and

state-of-charge (SOC) data using regression analysis, Laplace transfer s-domain transfer function development for charge and discharge. The results of the current work are unique in the framework taken, i.e., the transfer functions are obtained from curve-fits for the transient performance of the system, in contrast to deriving the transfer functions via the control algorithm as done in archival studies. The body of the paper describe the test apparatus, charging and discharging data collection, solar insolation modelling, SIMULINK model for charging and discharging stages, comparison of charging and discharging with and without the use of charge controller, development of transfer function models for charging and discharging stages followed by conclusions.

2 Test apparatus

The system being considered has the capability to study of the effects of using a charge controller on the performance of the PV system. The system test apparatus is composed of an array of six identical solar panels, two identical batteries, and a load. The load is a DC powered electric water pump. For safety purposes, only one PV panel and one battery were used to collect the data presented herein. Figure 1 shows the system under test. The inputs into the charge controller are the voltage and current that comes from the solar panel, before they are modified by the controller. The outputs from the charge controller are the voltage and current that go into the battery. The controller employs an internal data logger equipped with a memory card, which records the battery voltage, current, and SOC. The load tied to the battery used in the experiment was a DC pump. Three panels can be connected in parallel to charge a battery, which will provide power for the pump. The other three panels can also be connected in parallel, but with a charge controller to modulate energy storage in the battery. Again we emphasise here that for safety reasons, only one PV panel was used and only one battery was charged and discharged. The solar panels used are 'Hyundai 260 W 60 cell Poly Black Frame', HIS-M260RG-BF. The electric output of this panel has a nominal power output P_{mpp} =260 W, a voltage of V_{mpp} = 31.1 V and an amperage of I_{mpp} = 8.4 A. where mpp denotes maximum peak to peak. The batteries used are Aquion Aspen 24V Battery 83Ah, AQ-24S-83. The Aspen 24S-83 battery is based on saltwater. It contains manganese oxide as the cathode, carbon titanium phosphate composite as the anode, and alkali-ion saltwater as the electrolyte. The nominal voltage of the battery is 24V, and nominal capacity is 83 Ah. The charge controllers used are the STECA-TAROM 4545-48 model. They employ PWM control. The STECA-TAROM 4545-48 charge controlled can operate on batteries of 12/24/48 V. It can admit a maximum voltage of 100 V, and maximum current of 45 A from the PV array. The performance of the system is tested with both charge controllers. The first step is to test the PV system using the TAROM 4545-48 controller. Three panels in parallel are connected to the controller, battery, and the pump. The performance of the electric system is then recorded with and without the controller. The empirical load of the system was the water pump shown in Figure 4. The pump of Figure 4 has normal operating voltage of 24 V, and normal operating current of 3.0 A.

Figure 1 Photovoltaics panels under test (see online version for colours)

Figure 2 Batteries in battery enclosure (see online version for colours)

Figure 3 Charge controller used during test (see online version for colours)

Figure 4 Water pump used for the system load (see online version for colours)

3 Experimental charging data collection

The study of the effects of using a charge controller on the performance of the PV system was composed of a single PV panel, one battery, and a load. The load used is a DC powered electric water pump. This pump is connected to a bucket of water to circulate the water in a closed loop. The goal of the load is to discharge the battery. At first, one solar panel will charge the battery through the charge controller. After the battery is fully charged, the panel is disconnected, and the load is connected. The load will remain connected until the battery is fully discharged. The data from the controller was taken and recorded on an EXCEL file. Figure 5 shows the typical data format obtained. The charge controller has an internal data logger which records battery voltage, charge current, load current, and SOC of the battery over the time of operation. The controller has a micro SD card port (memory stick), which can store the data needed. The battery on the roof of the engineering building was charged on 9 May 2018 in Pomona, CA, USA. The battery was at 10% SOC. Charging of the battery began at 12:00 noon on 9 May 2018 and continued until 10 May 2018 until it was fully charged. Figures 6, 7 and 8 show plots of the voltage, current and SOC experimental data, respectively. When the experimental apparatus is executed, the values of the battery voltage and current are the same as that of the load, since the controller forces the voltage across the battery and load to be the same and regulates the current to a constant value throughout the discharging process. The controller also has a deep discharge protection option, which does not allow the battery to fully discharge to 0%. The lowest value possible of the deep discharge option was 10%, thus we chose that option to study the performance of the battery from 100% SOC, to 10% SOC. Herein, we adopted the threshold setting of 10% for our experimental data collection and thus the SOC terminates at a minimum of 10%, and does not go below it. Note from Figure 7, it can be seen at 20 hrs = 72,000 sec the time take to charge the battery has been reached, while the time corresponding to 100,000 sec is where the memory card was removed from the charge controller corresponding to a SOC = 100%, since the battery was no longer charging. Thus the plateau shown from approximately 90,000 sec to 100,000 sec in Figure 8 is witnessed, what the charge controller prevents the battery from being overcharged.

Figure 5 Excel file of data from charge controller

Steca Elektronik	Tarom 4545-48	758595CC006258760045		
Date	Time	Vbat[V]	SOC[%]	Ipv[A]
09-05-18	11:56:40	25.48	11	8.5
09-05-18	11:57:40	25.56	11	8.5
09-05-18	11:58:39	25.59	11	8.5
09-05-18	11:59:39	25.59	11	8.5
09-05-18	12:00:39	25.62	11	8.5
09-05-18	12:01:39	25.63	12	8.5
09-05-18	12:02:39	25.65	12	8.5
09-05-18	12:03:39	25.65	12	8.5
09-05-18	12:04:39	25.67	12	8.5
09-05-18	12:05:39	25.68	13	8.5
09-05-18	12:06:38	25.7	13	8.4
09-05-18	12:07:38	25.71	13	8.4
09-05-18	12:08:38	25.73	13	8.5
09-05-18	12:09:38	25.75	13	8.5
09-05-18	12:10:38	25.76	14	8.5

Figure 6 Voltage vs. time data collection (see online version for colours)

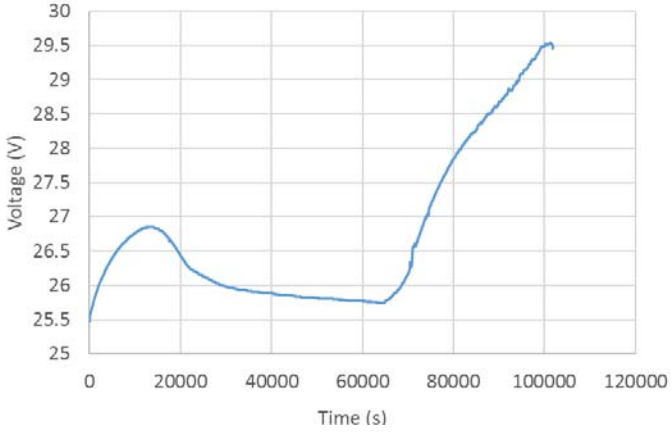

Figure 7 Photovoltaic current vs. time data collection (see online version for colours)

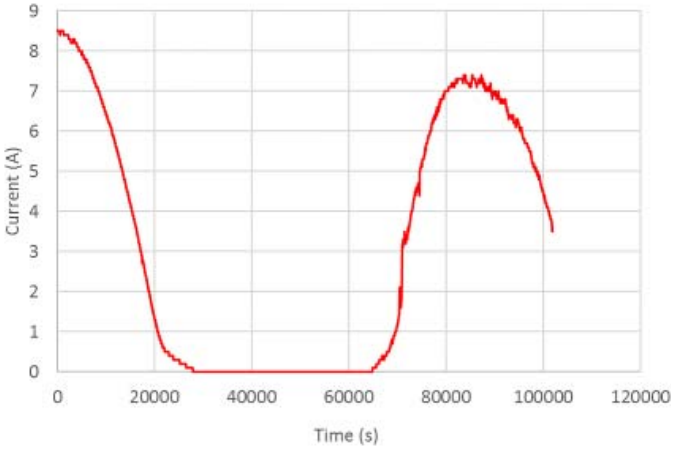

Figure 8 SOC vs. time data collection (see online version for colours)

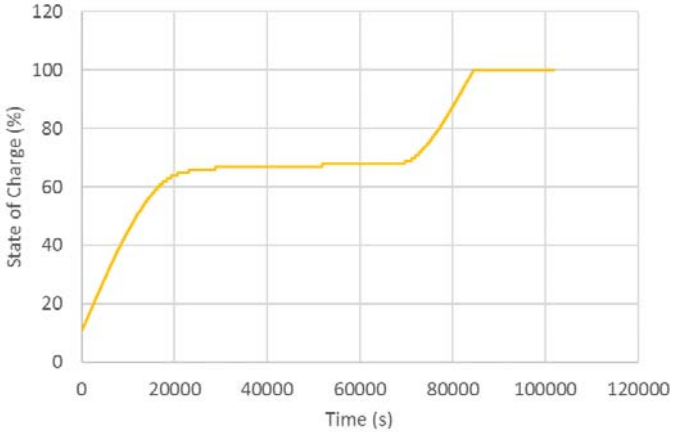

4 Experiments discharge data collection

After the battery was charged, it was connected to a pump and operated until the battery reached 10% SOC. The controller does not allow the battery to be fully discharged, the minimum allowable SOC to be reached during discharge is 10%. The data was obtained from the controller and plotted on EXCEL. The battery was fully charged (100% SOC), and continued to operate until it reached 10% SOC. The results are plotted in Figure 9, 10, and 11 for voltage, current and SOC, respectively. Note, from Figure 9, the sharp discontinuity at 80,000 sec is where the deep discharge protection feature of the charge controller is enacted, i.e., 10% SOC opens the circuit and resets the voltage to approximately 24.5 V. This is also shown in Figure 10, where the current goes from 3 A to 0 A at 80,000 sec, and in the SOC curve of Figure 11, where the SOC is shown to plateau at a constant value after 80,000 sec. The SOC reaches 10% at around 80,000 seconds, after that point, the controller opens the circuit and restores the voltage to 25 V. This is the deep discharge protection of the controller. After that point, the current is zero, and the SOC remains at 10%. The current operates at a constant value of approximately 3.3 A. The voltage and SOC will be plotted and correlated for time between 0 and 80,000, right before the intervention of the controller. The second part will be modelled separately. A closer look at the graphs of voltage and current, shows that they appear to decrease in steps. This is due to the controller allowing power to pass in pulses, when the pulse is non-zero, the voltage and SOC decrease, when the pulse is zero, both remain constant until the next cycle begins.

Figure 9 Discharge process voltage vs. time data collection (see online version for colours)

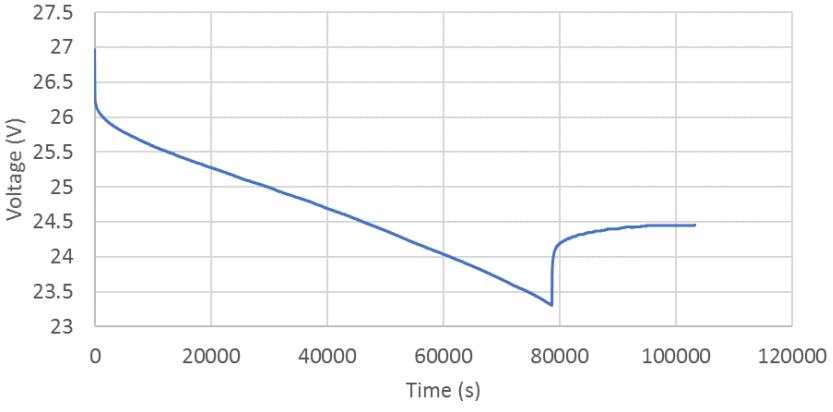

Figure 10 Discharge process current vs. time data collection (see online version for colours)

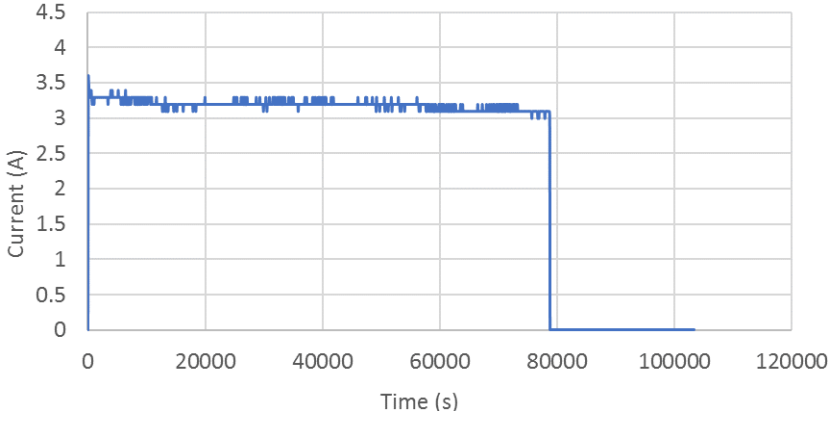

Figure 11 Discharge process SOC vs. time data collection (see online version for colours)

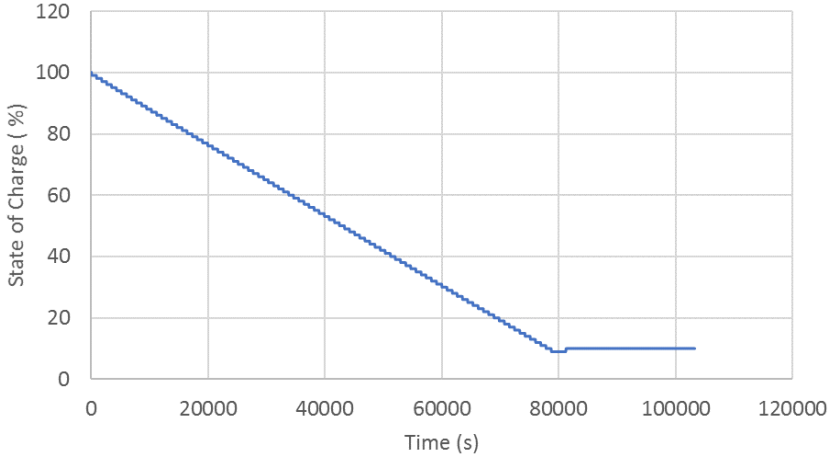

5 Solar insolation modelling

In order to model the charging process of the system, the solar insolation needed to be known. The solar insolation was modelled using the NREL PVWatts program. Figure 12 shows the insolation model. For purposes of modelling the charging process in a series of events, the insolation curve has been divided into 3 discrete time regions as shown in Figure 12.

Figure 12 Model of solar insolation used as forcing function of the system model (see online version for colours)

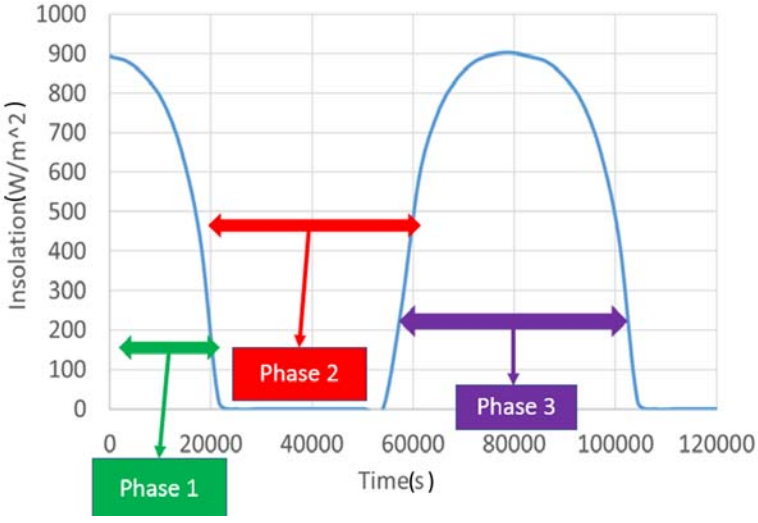

6 System modelling for charging

In order to compare the results of charging the battery with and without the controller, we must have data for voltage and current for charging the battery with no controller. Unfortunately, due to safety hazards, we cannot connect the panel on the roof directly to the battery and measure the voltage and current throughout the charging process. Instead, the battery will be charged with the panel on Simulink, and the results obtained will become the data that will be used for comparison with those from the controller obtained from the charging process. Figure 13 shows the Simulink model used for the charging process. The details of the Simulink programs presented herein can be found in Anderson and Yassine (2019). Figure 14 and Figure 15 show the simulated voltage and current output from the charging SIMULINK model, respectively. As seen from Figure 14 and Figure 15, the voltage and current across the panel are in the same phase as the insolation. Thus, the voltage and current are correlated for the same phase as done with the insolation profile.

Figure 13 Charging SIMULINK model (see online version for colours)

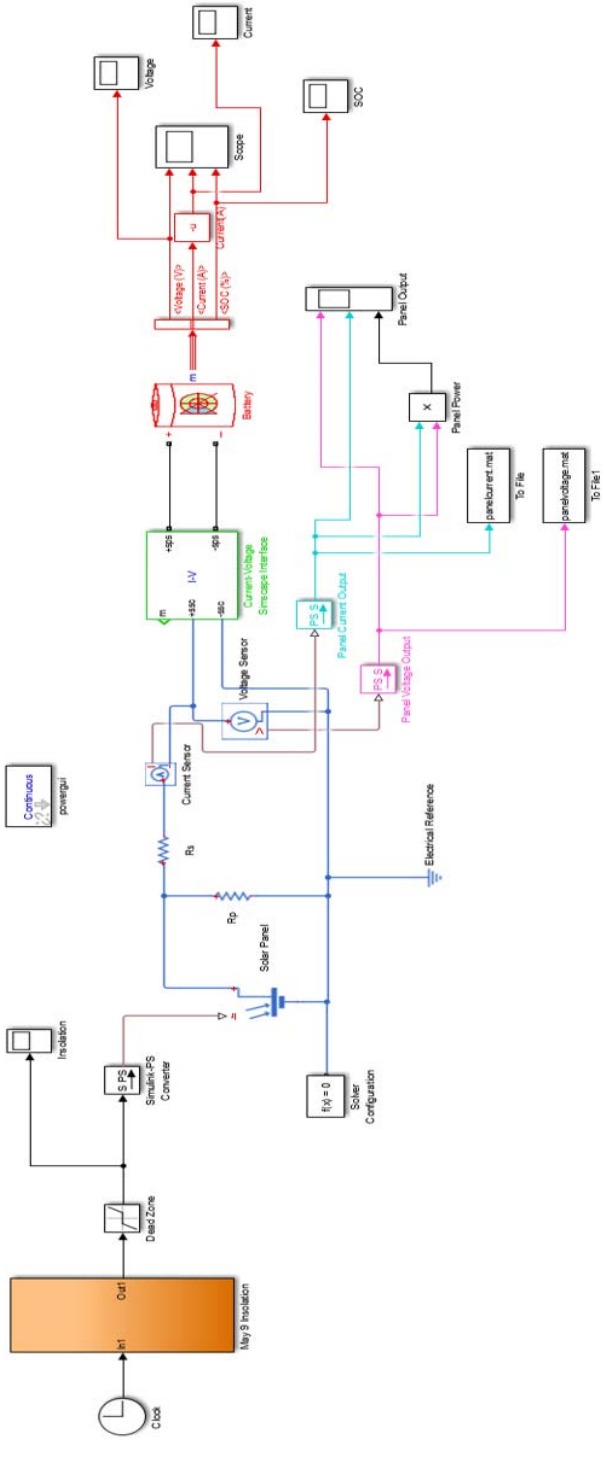

Figure 14 Charging SIMULINK model voltage prediction (see online version for colours)

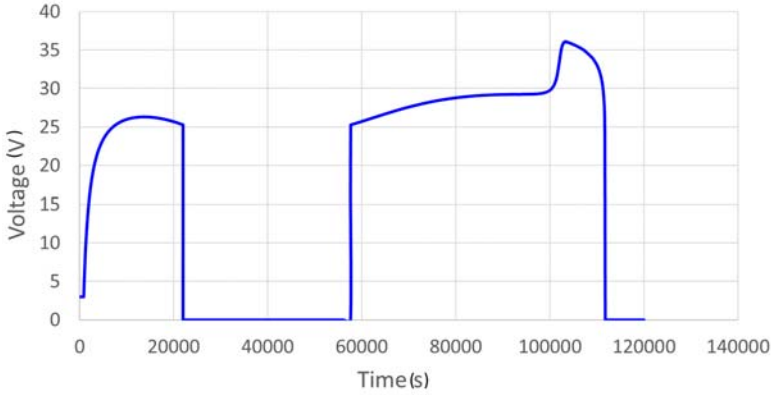

Figure 15 Charging SIMULINK model current prediction (see online version for colours)

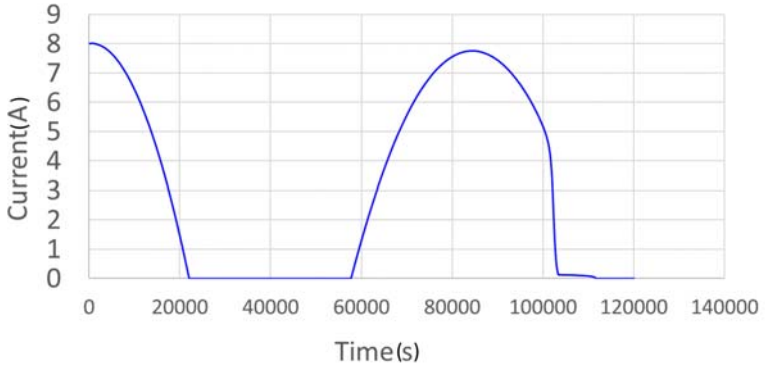

7 Comparison of charging with and without charge controller

In order to quantify the effect of charge control on the system performance, a simulation was performed without the charge controller enabled. The datasets without the charge controller enabled are plotted on the same graph for comparison as shown in Figure 16. As can be noted from Figure 16, the controller does not allow the sudden drop or rise of voltage. Also, the controller voltage varies between 25.5 and 29.5 V over the entire time span, while the voltage without the controller varies between 35 and 0 V. This offers clarification as to how the controller regulates the voltage across the panel/battery. The reason the voltage stays close to 26 V is that the controller is set to float charge the battery at 25 V. Float charging is defined as charging the battery over a long period of time with a low voltage. Figure 17 shows the comparison between controller current profile with controller (red line) and panel current without controller (blue line). From Figure 17, the battery current in both cases are similar. The slight difference is that the controller current is delayed from 57,600 to 66,000 seconds, which is about 2.3 hours,

this is related to the functioning of the charge controller. Figure 18 shows the plot of the SOC with (gold yellow line) and without (green line) the use of the charge controller. The SOC curves for both cases have similar slopes during the charging phases, however there is an offset between the two. The reason for this offset is due to the controller's boost charge function, which automatically starts when the SOC of the battery is 40%. The boost charge supplies a voltage of 28 V to the battery, which causes the offset difference between the two curves. Unfortunately, this option cannot be turned off.

Figure 16 Comparison between controller voltage profile (blue line) and panel voltage without controller (orange line) (see online version for colours)

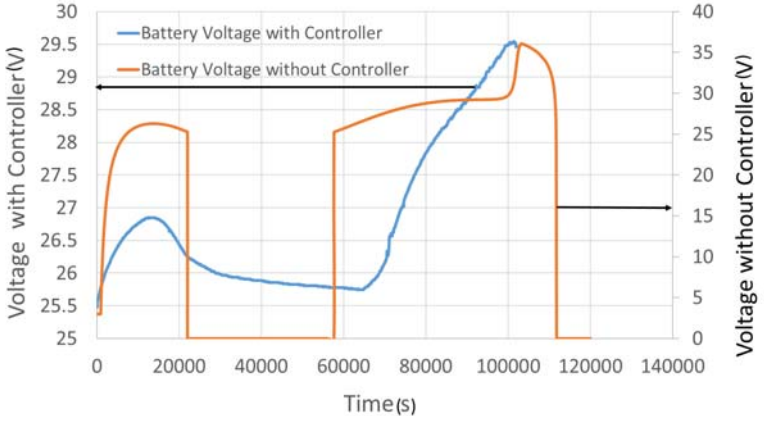

Figure 17 Comparison between controller current profile with controller (red line) and panel current without controller (blue line) (see online version for colours)

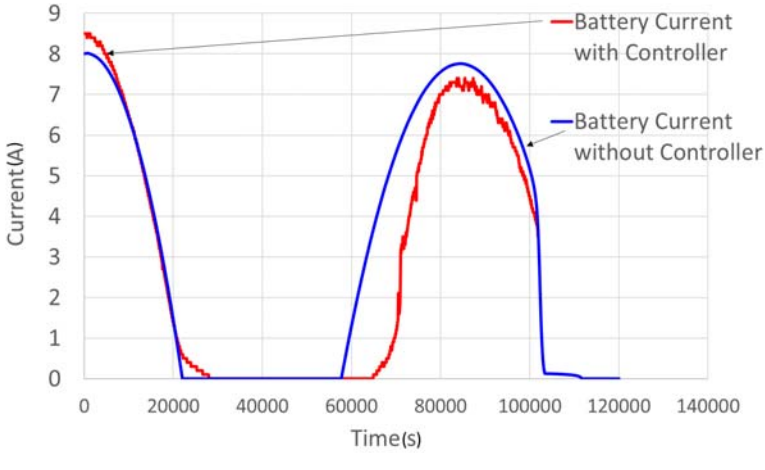

Figure 18 Comparison between controller SOC profile with controller (gold yellow line) and SOC without controller (green line) (see online version for colours)

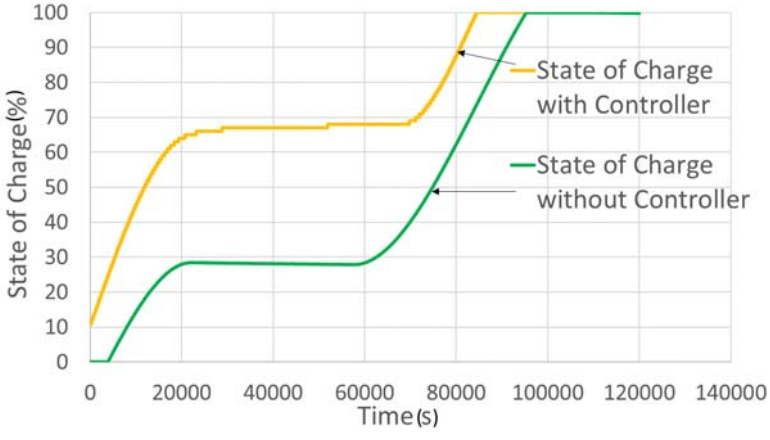

8 System modelling for battery discharging

The Simulink model for discharging is shown in Figure 19. The Simulink model shown in Figure 19 represents a battery connected to a resistor, which represents the pump as a load. The average resistance of the pump is 8 Ω, thus the 'R block' in red has the value of 8 Ω. The battery parameters are recorded on the scope and EXCEL. The voltage and current for the battery are the same for the resistor (pump). Figures 20, 21, and 22 show the voltage, current and SOC as functions of time, repectively from the discharge model simulation prediction.

Figure 19 Battery discharging SIMULINK model (see online version for colours)

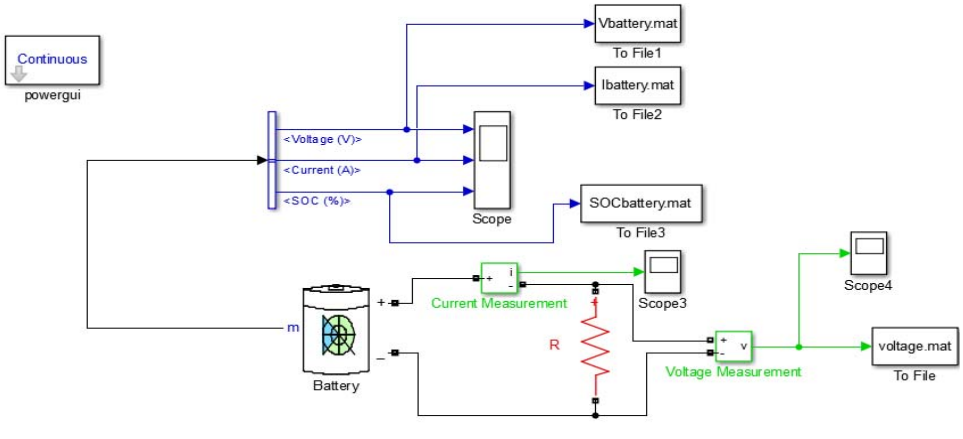

From above, the voltage and current are exactly similar in profile, where the current is 1/8 of the voltage, since the resistor is a linear element which causes the current to be proportional to the voltage from Ohm's Law, V = IR, with R = 8 Ω. At the point of 100,000 seconds, the voltage and current sharply decrease. This is the breakdown region of the battery, where it is almost fully discharged. The SOC at this point is about 5%, which is almost zero energy left in the battery. Since the values of the parameters with the controller are all above 10%, the values for this simulation below SOC = 10% will be ignored in the correlation of the parameters. When simulating the discharge of the battery without the controller, the voltage and current curves have the same profile. The SOC curve appears to be linearly decreasing, but that does not mean that the current and voltage must be exactly linearly decreasing as well. The SOC curve appears linear since the energy from the battery is being consumed at a steady rate throughout the majority of the duration. The voltage and current curves have the same profile since the load (DC pump) is modelled as a resistor of 8 ohm. Thus V = R*I, the current curve is equivalent to the voltage curve divided by 8. From 0 to 80,000 seconds, the voltage and current follow a linear trend. But after 80,000 seconds, the battery's voltage enters its breakdown region, since its SOC is too low, that is why the voltage and current show a sharp downward curve. Note from Figure 20 and Figure 21 at 80,000 sec, the breakdown region of the battery can be seen, where the linear slope from 0 to 80,000 sec suddenly becomes nonlinear.

Figure 20 Battery discharging SIMULINK model voltage prediction (see online version for colours)

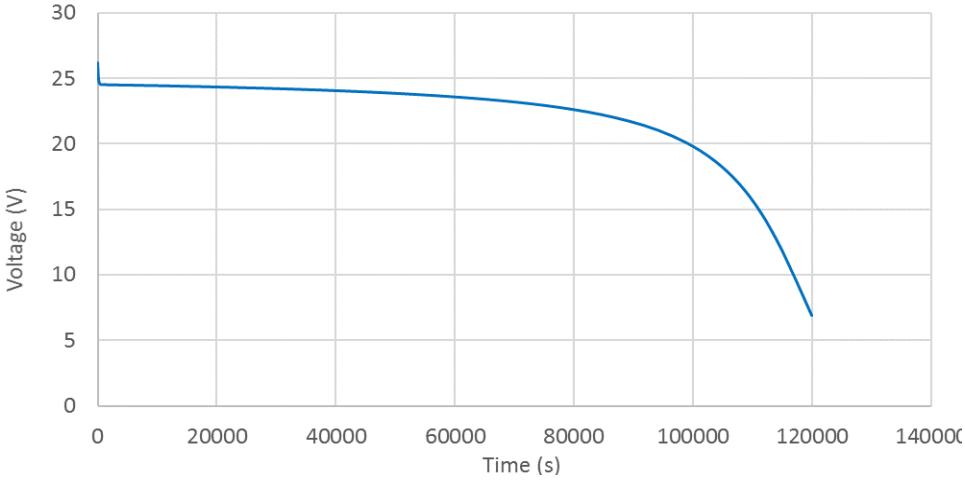

Figure 21 Battery discharging SIMULINK model current prediction (see online version for colours)

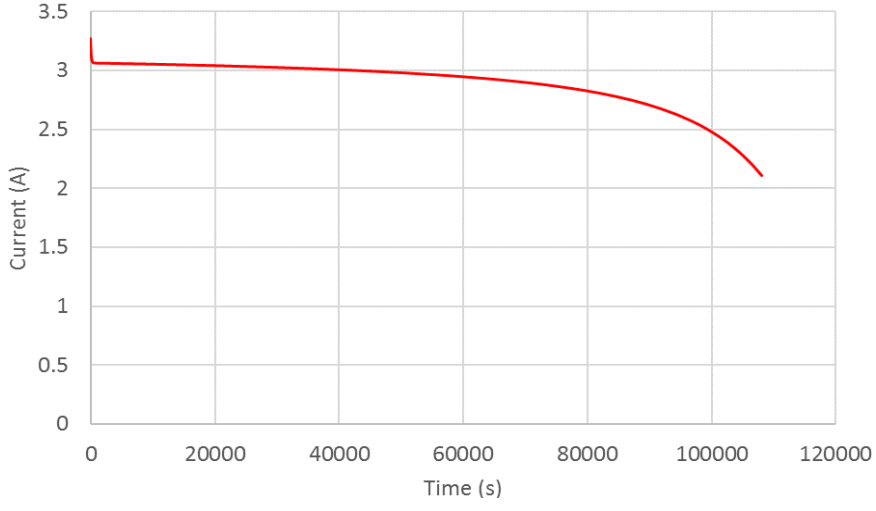

Figure 22 Battery discharging SIMULINK model SOC prediction (see online version for colours)

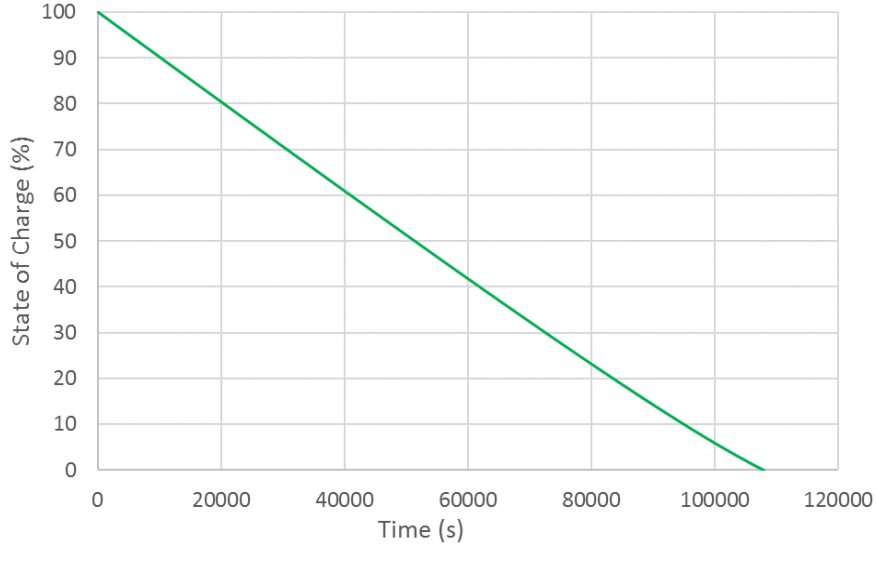

9 Comparison of discharging with and without charge controller

The curves of the two discharging processes will be plotted on the same graph for comparison as shown in Figures 23, 24 and 25 for voltage, current and SOC, respectively. As seen from Figure 23, the voltage of the battery with the controller stays close to 25 V. It does not go below 24 V. The controller keeps the voltage in a certain range. Meanwhile, the voltage of the battery without the controller drops below 10 V. There are

no limits on the voltage drop in the case of no controller. From Figure 24, the current in the controller ranges only from 3.4 A to 3.2 A. Its average is 3.3 A which remains constant until the battery reaches SOC of 10%, at which it becomes zero. For the current without controller the battery behaves like the voltage, where it keeps dropping until the battery is empty. There are no limits on the current drop in the case of no controller. From Figure 25, we observe that the SOC curve with the controller drops in steps, due to the 'on-off' functioning of the controller. This curve is steeper than that of not using the controller. This is since the voltage and current are made to be almost constant at values higher than those that would be without the controller.

Figure 23 Comparison between battery discharge voltage with controller (blue line), and without controller (orange line) (see online version for colours)

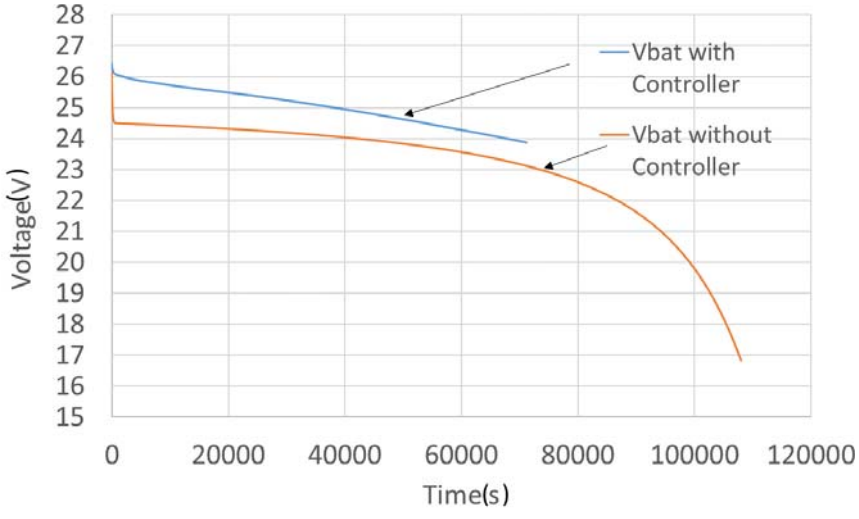

Figure 24 Comparison between battery discharge current with controller (blue), and without controller (orange) (see online version for colours)

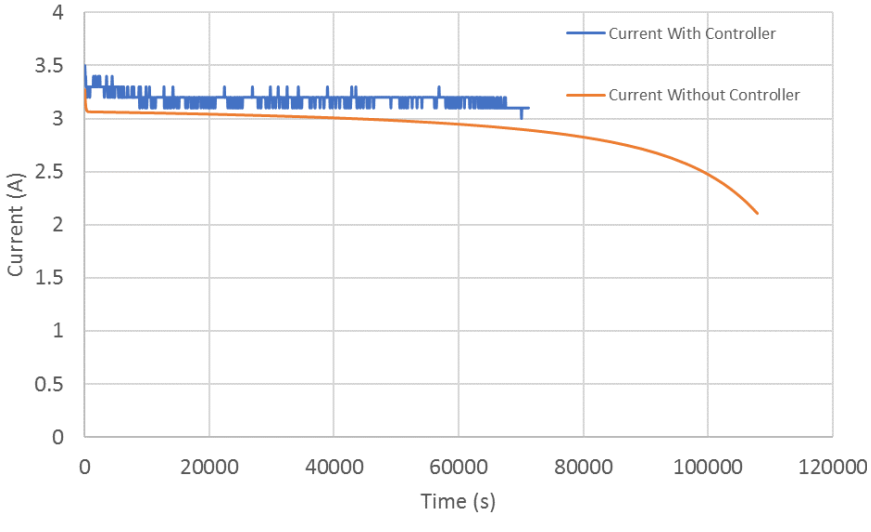

Figure 25 Comparison between battery discharge SOC with controller (blue), and without controller (orange) (see online version for colours)

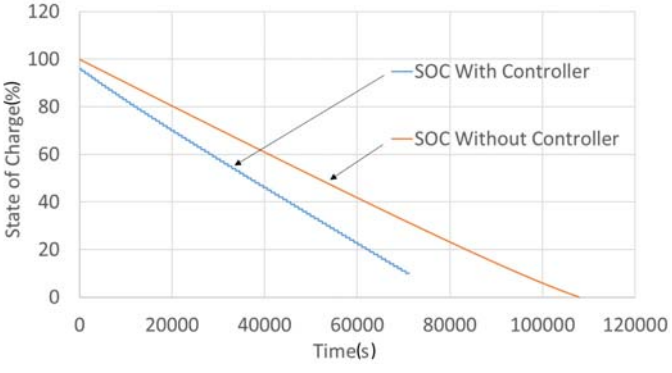

10 Transfer function modelling for charging

In this section of the paper, we present the development of transfer functions in Laplace space for the charging and discharging of the system. After correlating the voltages and currents as functions of time using regression and the actual test data, the transfer functions, which characterise the charge controller, will be obtained. This is done by applying the Laplace Transform to the voltage and current parameters, and dividing the Laplace Transform of the controller parameter by the panel parameter. Herein, s denotes the Laplace frequency while the coefficients in the numerator coefficients and denominator of the transfer functions denote the residues for the poles and zeros of the system. This is shown generically for the transfer function of equation (1).

$$\frac{N(s)}{D(s)} = \frac{a\exp(-t/\tau)(bs^2 + cs + d)}{(e + fs)(gs^2 + hs + l)} \tag{1}$$

where a is the magnitude; b, c, d, e, f, g, h, l are the residues of the system; and τ is a system time constant. The residues are invariant between time and Laplace frequency space and thus contain information about the system. In this case the transfer functions are formulated in order to export the system into a modelling environment such as MATLAB, GNU Octave, Scilab, etc., whereby each transfer function represents a physical component in the overall system. The poles and zeros are used to determine the stability map of the system. The various parameters in the transfer functions shown herein are the magnitudes of the poles and zeroes of the system. The time functions of the panel voltage and current in their respective phases are listed below for the following regions of time (as defined in Figure 13). Here the Heaviside unit step function $U(t)$ is used.

$$\begin{aligned} &\text{Phase 1: } 0 < t \le 22{,}000 \text{ sec} \\ &\text{Phase 2: } 22{,}000 < t \le 57{,}600 \text{ sec} \\ &\text{Phase 3: } 57{,}600 < t \le 85{,}000 \text{ sec} \end{aligned} \tag{2}$$

- Phase 1:

$$V = \left(3 + 23\left(1 - \exp(t/2400)\right)\right) \cdot U(t)$$
$$I(t) = \left(-2\times10^{-8}t^2 + 2\times10^{-5}t + 8\right) \cdot U(t) \tag{3}$$

- Phase 2:

$$V = 0 \cdot U(t - 22{,}000)$$
$$I(t) = 0 \cdot U(t - 22{,}000) \tag{4}$$

- Phase 3:

$$V = (0.0001t + 17.582) \cdot U(t - 57{,}6000)$$
$$I(t) = (-1\times10^{-8}t^2 + 0.00018t - 69.543) \cdot U(t - 57{,}600) \tag{5}$$

Taking the Laplace transform of (3), (4) and (5) affords

- Phase 1:

$$V(s) = 3\frac{s + 3.61\times10^{-3}}{s\left(s - 4.17\times10^{-4}\right)}$$
$$I(s) = 8\frac{s^2 + 2.5\times10^{-6}s - 5\times10^{-9}}{s^3} \tag{6}$$

- Phase 2:

$$V(s) = 0 * \exp(-22{,}000s)$$
$$I(s) = 0 * \exp(-22{,}000s) \tag{7}$$

- Phase 3:

$$V(s) = \frac{23.342\exp(-57{,}600s)(s + 4.3\times10^{-6})}{s^2}$$
$$I(s) = \frac{211\left(s^2 + 1.35\times10^{-5}s + 9.48\times10^{-11}\right)\exp(-57{,}600s)}{s^3} \tag{8}$$

Next, the time functions of the charge controller (experimental) parameters are listed below in their respective time phases

$$\begin{aligned}&\text{Phase 1: } 0 < t \le 22{,}000 \text{ sec}\\ &\text{Phase 2: } 22{,}000 < t \le 66{,}000 \text{ sec}\\ &\text{Phase 3: } 66{,}600 < t \le 85{,}000 \text{ sec}\end{aligned} \tag{9}$$

- Phase 1:

$$V(t) = \left(-8\times10^{-9}t^2 + 0.0002t + 25.621\right) \cdot U(t)$$
$$I(t) = \left(-2\times10^{-9}t^2 - 0.0003t + 9.3782\right) \cdot U(t) \tag{10}$$

- Phase 2:

$$V(t) = (4\times10^{-10}t^2 - 4\times10^{-5}t + 26.8)\cdot U(t-22{,}000)$$
$$I(t) = 0\cdot U(t-22{,}000) \tag{11}$$

- Phase 3:

$$V(t) = (0.0001t + 19.126)\cdot U(t-66{,}000)$$
$$I(t) = (-2\times10^{-8}t^2 + 3.4\times10^{-3}t - 137.2)\cdot U(t-66{,}000) \tag{12}$$

Taking the Laplace transform of (10), (11) and (12) affords

- Phase 1:

$$V(s) = \frac{25.621s^2 + 0.0002s - 1.6\times10^{-8}}{s^3}$$
$$I(s) = 9.3782\frac{s^2 - 3.2\times10^{-5}s - 4.3\times10^{-10}}{s^3} \tag{13}$$

- Phase 2:

$$V(s) = \frac{26.1\left(s^2 - 8.6\times10^{-7}s + 3.1\times10^{-11}\right)\exp(-22{,}000s)}{s^3}$$
$$I(s) = 0 \tag{14}$$

- Phase 3:

$$V(s) = \frac{25.726\exp(-66{,}000s)(s + 3.9\times10^{-6})}{s^2}$$
$$I(s) = \frac{174.32(s^2 + 3.5\times10^{-5}s + 2.3\times10^{-19})\exp(-66{,}000s)}{s^3} \tag{15}$$

The transfer functions for voltage and current will be obtained by dividing the output signal by the input signal. Where the output signal is the experimental signal given by equations (13), (14), (15), respectively and the input signal is the real signal given by equations (5), (6), (7), respectively. Thus, the voltage and current transfer functions are determined to be as follows, where G(s) is the voltage transfer function, and H(s) is the current transfer function, respectively.

- Phase 1:

$$G(s) = \frac{8.54033(s^3 + 4.281\times10^{-4}s^2 + 2.633\times10^{-9}s - 2.602\times10^{-13})}{s^3 + 0.00361s^2}$$
$$H(s) = \frac{1.17(s^2 - 3.2\times10^{-5}s - 4.3\times10^{-10})}{s^2 + 2.5\times10^{-6}s - 5\times10^{-9}} \tag{16}$$

- Phase 2:

$$G(s) = 0 \text{ (no insolation)}$$
$$H(s) = 0 \text{ (no output)} \tag{17}$$

- Phase 3:

$$G(s) = \frac{1.102(s + 3.9\times10^{-6})\exp(-8400s)}{s + 4.3\times10^{-6}}$$
$$H(s) = \frac{0.83(s^2 + 3.5\times10^{-5}s + 2.3\times10^{-10})\exp(-8400s)}{s^2 + 1.35\times10^{-5}s + 9.48\times10^{-11}} \quad (18)$$

The stability characteristics of the transfer functions for charging are summarised in Table 1.

Table 1 Stability characteristics of charging transfer functions

Transfer function for charging			
	Transfer function	*Poles*	*Zeroes*
Voltage phase 1	$\frac{8.54033 * (s^3 + 4.281 * 10^{-4} * s^2 + 2.633 * 10^{-9} * s - 2.602 * 10^{-13})}{s^3 + 0.00361 s^2}$	$s_1 = 0, s_2 = 0$ $s_3 = -0.00361$	$s_1 = -4.2 * 10^{-4}$ $s_2 = 2.13 * 10^{-5}$ $s_3 = -2.9 * 10^{-5}$
Voltage phase 3	$\frac{1.102 * (s + 3.9 * 10^{-6}) * \exp(-8,400s)}{s + 4.3 * 10^{-6}}$	$s_1 = -4.3 * 10^{-6}$	$s_1 = 3.9 * 10^{-6}$
Current phase 1	$\frac{1.17 * (s^2 - 3.2 * 10^{-5} * s - 4.3 * 10^{-10})}{s^2 + 2.5 * 10^{-6} * s - 5 * 10^{-9}}$	$s_1 = -6.95 * 10^{-5}$ $s_5 = -7.2 * 10^{-5}$	$s_1 = 4.22 * 10^{-5}$ $s_2 = -1.02 * 10^{-5}$
Current phase 3	$\frac{0.83 * (s^2 + 3.5 * 10^{-5} * s + 2.3 * 10^{-10}) * \exp(-8,400s)}{s^2 + 1.35 * 10^{-5} * s + 9.48 * 10^{-11}}$	$s_1 = -6.75 * 10^{-6} + 70.017 * 10^{-6}i$ $s_2 = -6.75 * 10^{-6} - 70.017 * 10^{-6}i$	$s_1 = -8.77 * 10^{-6}$ $s_2 = -2.62 * 10^{-5}$

11 Transfer function modelling for discharging

The discharging process is a bit simpler to model than charging. The parameters obtained for discharging the battery will be listed again for completeness. Actual discharge parameters before entering the charge controller are taken from correlation of discharge data

$$V(t) = -4\times10^{-5}t + 25.718$$
$$I(t) = -5\times10^{-6}t + 3.2148 \quad (19)$$

Note from equation (19) that the trend is a linear curve with a very small negative slope which is consistent with the trends shown in Figure 20 and Figure 21, respectively. The small slope in voltage and current is consistent with the empirical data.

Next, the experimental discharge parameters (after controller takes effect) are given by

$$V(t) = -3\times10^{-5}t + 25.96$$
$$I(t) = 3.3 \quad (20)$$

Taking the Laplace transform of (19) and (20) yield

Real discharge:

$$V(s) = \frac{25.718(s - 1.56\times10^{-6})}{s^2}$$
$$I(s) = \frac{3.2148(s - 1.56\times10^{-6})}{s^2} \tag{21}$$

Experimental discharge:

$$V(s) = \frac{25.96(s - 1.16\times10^{-6})}{s^2}$$
$$I(s) = \frac{3.3}{s} \tag{22}$$

The transfer functions for the discharging process are now determined by taking the ratio of equation (21) and equation (22), thus

$$G(s) = \frac{1.01(s - 1.16\times10^{-6})}{s - 1.56\times10^{-6}}$$
$$H(s) = \frac{1.027s}{s - 1.56\times10^{-6}} \tag{23}$$

The stability characteristics of the transfer functions for charging are summarised in Table 2.

Table 2 Stability characteristics of discharging transfer functions

Transfer function for discharging			
	Transfer function	*Poles*	*Zeroes*
Voltage	$\frac{1.01(s - 1.16\times10^{-6})}{(s - 1.56\times10^{-6})}$	$s_1 = 1.56 * 10^{-6}$	$s_1 = 1.16 * 10^{-6}$
Current	$\frac{1.027 * s}{s - 1.56 * 10^{-6}}$	$s_1 = 1.56 * 10^{-6}$	$s_1 = 0$

12 Conclusions

This paper has presented the development and fabrication of a test apparatus for PV/battery storage/charge controlling using manganese oxide/carbon titanium phosphate composite/alkali-ion saltwater electrolyte battery cells for energy storage. The paper presents the hardware of test apparatus, charging and discharging data collection, solar insolation modelling, SIMULINK model for charging and discharging stages, comparison of charging and discharging with and without the use of charge controller, development of transfer function models for charging and discharging. The key take-away points from this paper are as follows:

1 Construction and assembly of practical hardware of a test facility of PV/battery storage/charge controlling research and development has been presented.

2 The charge controller has an internal data logger which records battery voltage, charge current, load current, and SOC of the battery over the time of operation.

3 For discharging, voltage and current transients appear to decrease in steps. This is due to the controller allowing power to pass in pulses, when the pulse is non-zero, the voltage and SOC decrease, when the pulse is zero, both remain constant until the next cycle begins.

4 During charging, the voltage and current across the PV solar panel are in the same phase as the insolation.

5 The controller voltage varies between 25.5 V and 29.5 V over the entire time span of data collection and simulation, while the voltage without the controller varies between 35 V and 0 V. The voltage stays close to 26 V is that the controller is set to float charge the battery at 25 V. Float charging is defined as charging the battery over a long period of time with a low voltage.

6 The SOC curves for both controlled and non-controlled have similar slopes during the charging phases, however there is an offset between the two. The reason for this offset is due to the controller's boost charge function, which automatically starts when the SOC of the battery is 40%. The boost charge supplies a voltage of 28 V to the battery, which causes the offset difference between the two curves.

7 The SIMULINK modelling indicates that the voltage and current are exactly similar in profile, where the current is 1/8 of the voltage, since the resistor (water pump) is a linear element which causes the current to be proportional to the voltage from Ohm's Law, $V = IR$, with $R = 8\ \Omega$. At the point of 100,000 seconds, the voltage and current sharply decrease. This is the breakdown region of the battery, where it is almost fully discharged. The SOC at this point is about 5%, which corresponds to having zero energy left in the battery.

8 Battery voltage with the controller enabled track close to 25 V. The battery voltage does not dip below 24 V. This is because the controller keeps the battery voltage in a certain range. In contrast, the battery voltage transients without the controller drop below 10 V. This is due to the fact that there are no limits on the voltage drop in the case of no charge controller.

9 The battery current with the controller enabled ranges only from 3.4 A to 3.2 A. Its average is 3.3A, and stays constant until the battery reaches SOC of 10%, at which it becomes zero. For the battery current without charge controller, the battery behaves like the voltage, where it keeps dropping until the battery is empty. There are no limits on the battery current drop in the case of no controller.

10 The battery SOC curve with the controller drops in steps, due to the 'on-off' functioning of the controller. This curve is steeper than that of not using the controller. This is since the voltage and current are made to be almost constant at values higher as opposed to the voltage and current trends without the controller.

11 Transfer function models have been developed from curve-fitted correlation experimental test data. These transfer function can be rolled out into a generic modelling framework for simulation of Manganese Oxide/Carbon Titanium Phosphate Composite/Alkali-ion Saltwater Electrolyte battery charging/discharging.

References

Abbes, D., Champenois, G., Martinez, A. and Robyns, B. (2013) 'Modeling and simulation of a photovoltaic system: an advanced synthetic study', *3rd International Conference on Systems and Control (ICSC)*, IEEE, pp.93–98.

Alvarez, G., Moradi, H., Smith, M. and Zilouchian, A. (2017) 'Modeling a grid-connected pv/battery microgrid system with MPPT controller', *IEEE 44th Photovoltaic Specialist Conference (PVSC)*, IEEE, pp.2941–2946.

Amor, W.O., Amar, H.B. and Ghariani, M. (2015) 'Economic and technical approach for a grid connected to PV power system', *International Journal of Energy, Environment and Economics*, Vol. 23, No. 6, p.699.

Anderson, K.R. and Yassine, W. (2019) 'Simulink modelling of a solar PV battery PWM controller apparatus', *ICEAS 2019 The 9th International Conference on Engineering and Applied Science*, Hilton Waikiki Beach, Oahu, Hawaii, USA, 6–8 August.

Barote, L., Weissbach, R., Teodorescu, R., Marinescu, C. and Cirstea, M. (2008) 'Stand-alone wind system with vanadium redox battery energy storage', *11th International Conference on Optimization of Electrical and Electronic Equipment, 2008. OPTIM 2008*, IEEE, pp.407–412.

Bellia, H., Youcef, R. and Fatima, M. (2014) 'A detailed modeling of photovoltaic module using MATLAB', *NRIAG Journal of Astronomy and Geophysics*, Vol. 3, No. 1, pp.53–61.

Cai, H., Xiang, J. and Wei, W. (2016) 'Modelling, analysis and control design of a two-stage photovoltaic generation system', *IET Renewable Power Generation*, Vol. 10, No. 8, pp.1195–1203.

Chen, C.L., Lai, J.S., Martin, D., Wu, K.H., Ribeiro, P., Andrade, E., Liu, C., Lee, Y.S. and Yang, Z.Y. (2012) 'Modelling, analysis, and implementation of a photovoltaic grid-tie inverter system', *Twenty-Seventh Annual IEEE on Applied Power Electronics Conference and Exposition (APEC)*, IEEE, pp.1494–1501.

Das, S. and Akella, A.K. (2018) 'A control strategy for power management of an isolated micro hydro-PV-battery hybrid energy system', *4th International Conference on Electrical Energy Systems (ICEES)*, IEEE, pp.397–401.

Glavin, M.E., Chan, P.K., Armstrong, S. and Hurley, W.G. (2008) 'A stand-alone photovoltaic supercapacitor battery hybrid energy storage system', *13th Power Electronics and Motion Control Conference, 2008. EPE-PEMC 2008*, IEEE, pp.1688–1695.

Huang, B.J., Hsu, P.C., Wu, M.S. and Ho, P.Y. (2010) 'System dynamic model and charging control of lead-acid battery for stand-alone solar PV system', *Solar Energy*, Vol. 84, No. 5, pp.822–830.

Jariso, M., Khan, B., Tesfaye, D. and Singh, J. (2017) 'Modeling and designing of stand-alone photovoltaic system: case study: Addis Boder health center south west Ethiopia', *Electronics, Communication and Aerospace Technology*, Vol. 1, pp.168–173.

Miller, S. and Wendlandt, J. (2010) 'Real-time simulation of physical systems using Simscape', *MATLAB News and Notes*, pp.1–13.

Mirzaei, A., Forooghi, M., Ghadimi, A.A., Abolmasoumi, A.H. and Riahi, M.R. (2017) 'Design and construction of a charge controller for stand-alone PV/battery hybrid system by using a new control strategy and power management', *Solar Energy*, Vol. 149, pp.132–144.

Prakash, R. and Singh, S. (2016) 'Designing and modelling of solar photovoltaic cell and array', *IOSR Journal of Electrical and Electronics Engineering*, Vol. 11, No. 2, pp.35–40.

Shah, M.W. and Biate, R.L. (2016) 'Design and simulation of Solar PV model using MATLAB/Simulink', *International Journal of Scientific & Engineering Research*, Vol. 7, No. 3.

Shaw, P., Sahu, P.K., Maity, S. and Kumar, P. (2016) 'Modeling and control of a battery connected standalone photovoltaic system', *IEEE International Conference on Power Electronics, Intelligent Control and Energy Systems (ICPEICES)*, IEEE, pp.1–6.

Tazay, A. and Miao, Z. (2018) 'Control of a three-phase hybrid converter for a PV charging station', *IEEE Transactions on Energy Conversion*, Vol. 33, No. 3, pp.1002–1014.

Tsai, H.L., Tu, C.S. and Su, Y.J. (2008) 'Development of generalized photovoltaic model using MATLAB/SIMULINK', *Proceedings of the World Congress on Engineering and Computer Science*, pp.1–6.

Verma, K. and Gupta, A. (2016) 'A modeling and control functions of grid connected converter for solar photovoltaic system-a review', *7th India International Conference on Power Electronics (IICPE)*, IEEE, pp.1–6.

Yassine, W. (2018) *Characterization of a Photovoltaic System*, MSME Thesis, California State Polytechnic University at Pomona.